Journal of Science: Advanced Materials and Devices 5 (2020) 354–360

Contents lists available at ScienceDirect

Journal of Science: Advanced Materials and Devices

journal homepage: www.elsevier.com/locate/jsamd

Original Article

Giant magnetoelectric effects in serial-parallel connected Metglas/PZT arrays with magnetostrictively homogeneous laminates

Trinh Dinh Cuong [a], Nguyen Viet Hung [b], Vu Le Ha [a], Phung Anh Tuan [c], Do Dinh Duong [c], Ho Anh Tam [b], Nguyen Huu Duc [b], Do Thi Huong Giang [b, d, *]

[a] Institute of Electronic Academy of Military Science and Technology, Hanoi, Vietnam
[b] Laboratory for Micro-Nano Technology, VNU University of Engineering and Technology Vietnam National University, Hanoi, Vietnam
[c] School of Electrical Engineering, Hanoi University of Science and Technology, Hanoi, Vietnam
[d] Faculty of Engineering Physics and Nanotechnology, VNU University of Engineering and Technology, Vietnam National University, Hanoi, Vietnam

A R T I C L E I N F O

Article history:
Received 28 May 2020
Received in revised form
23 June 2020
Accepted 25 June 2020
Available online 3 July 2020

Keywords:
Magnetoelectric effect
Shape magnetic anisotropy
Shear-lag effect
Serial-parallel connection
Low magnetic field sensors

A B S T R A C T

To ensure the magnetostrictive softness, the homogeneity, the decrease of the shear-lag effect and the space-saving construction of narrowed longitudinal-transverse L-T magnetoelectric (ME) composites, a novel parallel-connected-multi-bars (PCMB) geometry of PZT/Metglas is proposed and investigated by simulation and experiment. In this case, Metglas layers are structured in different geometries from the conventional single bar (c-SB) to conventional separated multiple bars (c-SMB), elongated separate multi-bar (*e*-SMB) and n-magnetic-bar based PCMB (n-PCMB). This n-PCMB geometry divides the conventional ME configuration into *n* parallel-connected ME units (n-PCMEU) according to the magnetic geometries. The optimal ME performance with the largest ME voltage coefficient α_E of 630 V/cm.Oe is achieved in PCMEU with two Metglas bars (n = 2). The ME voltage coefficient can be further enhanced by integrating *m* of these optimal PCMEUs in series to form a serial-parallel ME unit array m-S (n-PMEU)A. The α_E value increases by a factor of 3.6 and reaches 2.238 kV/cm.Oe for 4-S (2-PMEU)A, a factor that is almost equal to m. The resulting 4-S (2-PMEU)A sensor possesses an extremely high sensitivity of 18.1 μV/nT, with a resolution of 10^{-1} nT.

1. Introduction

Magnetoelectric (ME) materials exhibit a coupling between ferroelectric and ferromagnetic order parameters. Such a coupling leads to the presence of electrically tunable magnetic parameters through a direct ME effect and develops an electric voltage under an externally applied magnetic field. This is in short the operational mechanism of ME sensors. The direct ME effect exists in single phase compounds as well as in composites and nano-micro interlayered structures. While both single phase multiferroic materials and multiferroic composites have attracted intense interests due to the expectation of strong ME coupling, the ME laminates have always been drawing considerable attention thanks to their simple design, low fabrication cost, high sensitivities and high temperature stability at room temperature [1–3]. This is the typical case for Tefenol-D/PZT [2,4], TefecoHan/PZT [5] and Metglas/PZT [1,6,7]. Indeed, the magnetic ME-laminate based sensors can function in the pico-Tesla (pT) range [8]. The highest ME coefficient of about 500 V/cm.Oe was found for an amorphous magnetostrictive FeBSiC alloy/piezofiber layered structure [9].

For ME laminates, attempts to increase the low magnetic field ME voltage response were mainly focused on the magnetic as well as the magnetotrictive softness of the magnetic phases. In this approach, highly magnetostrictive amorphous FeCoSiB (Metglas) and FeNiSiB foils are commonly applied [6,10–12]. In addition, simple sandwich ME geometries were designed with optimal magnetostriction/PZT volume fraction [13] and shapes [6,14–16]. Among them, the elongating mechanical ME shape (by increasing the ratio of the square of length (L^2) with respect to the product of thickness and width ($t.W$)) to strengthen the shape magnetic anisotropy of magnetostrictive layers has been successful in enhancing both the ME voltage and the ME sensor sensitivity. This

* Corresponding author. Laboratory for Micro-Nano Technology, VNU University of Engineering and Technology Vietnam National University, Hanoi, 10000, Viet Nam.
E-mail address: giangdth@vnu.edu.vn (D.T.H. Giang).
Peer review under responsibility of Vietnam National University, Hanoi.

https://doi.org/10.1016/j.jsamd.2020.06.005
2468-2179/

can be simply realized with magnetic layers of thin thickness, elongated length, and (or) narrowed width [7,17,18]. A successful approach, however, still faces to technical disadvantages. Firstly, in ME configurations with PZT and Metglas of the same size, the ME coupling is inhomogeneous due to the inhomogeneity of the magnetic induction distribution along the magnetostrictive Metglas layer. Secondly, narrowing the width faces to the edge effect called "shear-lagging" in the electrostrictive PZT layer [15,19]. Thirdly, the elongating is not suitable for sensor miniaturization.

To overcome the above mentioned disadvantages, in this work a novel integrated serial-parallel PZT/Metglas array is designed and investigated in the expectation to multiply the ME voltage response. It ensures a huge magnetostrictive softness as well as a diminishing shear-lag effect and space-saving. In particular, this ME array configuration could amplify the Signal-to-Noise Ratio (SNR) of the corresponding magnetic sensors.

2. Experimental

In Fig. 1, the sketch of the ME laminate configurations under investigation is illustrated. The melt-spun Metglas ribbon with 21 μm in thickness (t_m), acting as the piezomagnetic sensitive layers, was used thanks to its high magnetic and magnetostrictive softness. This ferromagnetic layer was assumed to be magnetized in the magnetic field applied along the length of the sample in the longitudinal direction (x-direction), while an out-of-plane (z-direction) polarization PZT ceramic plate with 500 μm in thickness (t_p) (855 American Piezoelectric company) [20] was used for strain mediated electric polarization. Hence the configuration of the ME composite considered here is L–T.

The PZT plate is chosen with large dimensions to lower the shear-lag effect, mentioned above. In this case, only the magnetic Metglas bars are narrowed and placed next to each other. This will divide the conventional ME configuration into parallel-connected units according to the magnetic geometry shown in Fig. 1a, bottom. By using the CNC technology (Bungard CCD/MTC, Germany), it was possible to precisely form both Metglas and PZT laminates in the designed configurations and sizes (Fig. 1b). The ME configurations consist of trilayers of the sandwich structure, in which the PZT with the fixed 50 mm in length (defined as sensing length L_s) and a variable width (W_p = 0.8–6 mm) was symmetrically bonded between two Metglas layers. To reach the research goal, here Metglas layers were structured in different geometries such as (i) the conventional single bar (c-SB) (n = 1) (top, Fig. 1a), (ii) conventional separated multiple bars (c-SMB) and (iii) elongated separate multi-bar (e-SMB) with the number of bars n = 2, 3, 4, 6, width w_m = 0.8 mm and the gap distance $\boldsymbol{g}$ = 0.35 mm (middle, Fig. 1a) and (iv) parallel-connected-multi-bars (PCMB or n-PCMB for the case of n magnetic bars) (bottom, Fig. 1a). This n-PCMB geometry divided the conventional ME configuration into n of parallel-connected ME units (n-PCMEU) according to the magnetic geometries. Note that, in the conventional geometries (i) and (ii), the length of the piezoelectric and piezomagnetic substances is kept the same as the sensing length L_s. In the elongated geometries (iii) and (iv), the length of the magnetic bars is increased with two elongated ends of the length e = 5 mm. As can be seen below, these elongated parts ensure the magnetostrictive homogeneity over the whole sensing part. At these two elongated ends, conjoined parts with the length c varying between 0 and 5 mm are designed in order to connect the magnetic bars in a parallel configuration. The pictures of these ME composite fabrication processes are given in Fig. 1b and c.

Moreover, in this investigation, the several (m) of PCMEUs can be connected in series, which fully establish an integrated serial-

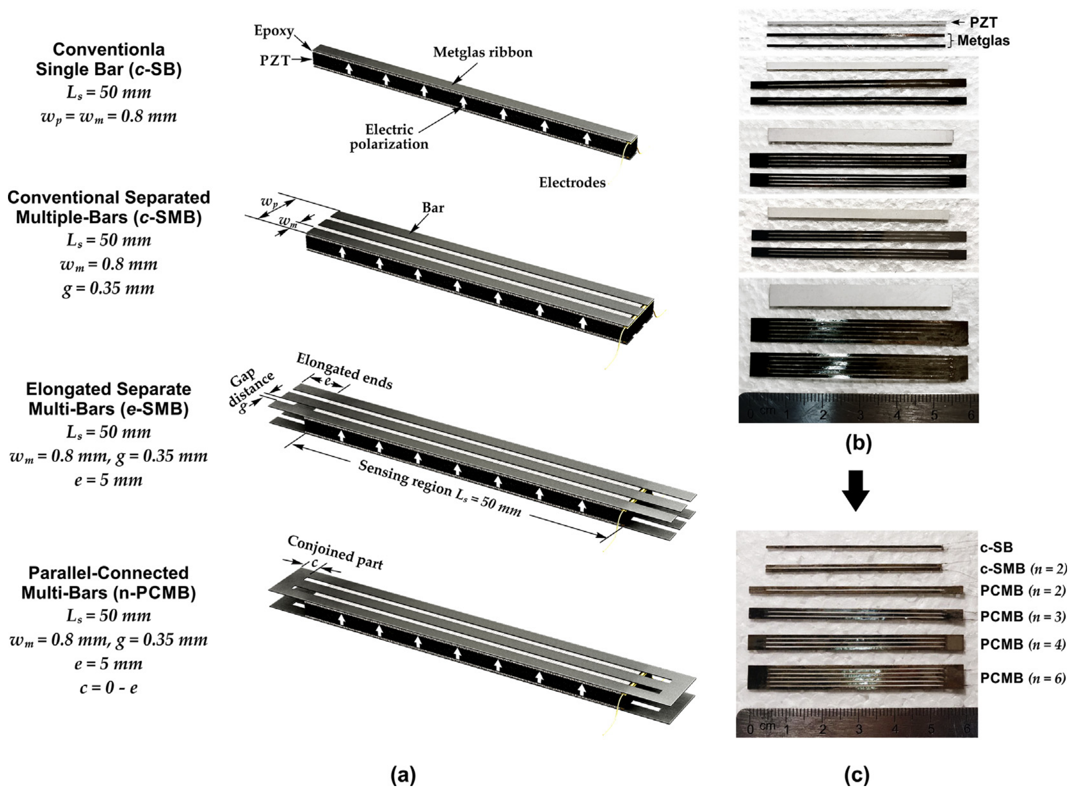

Fig. 1. (a) Schema of different ME geometries with conventional single (magnetic) bar (c-SB), separated multi-bars (c-SMB), elongated separate multi-bar (e-SMB) and parallel-connected-multi-bar (n-PCMB), (b) images of manufactured Metglas and PZT components and (c) manufactured ME laminate composites.

parallel Metglas/PZT array with magnetostrictive homogeneous laminates. For short, this novel structure of the ME laminate array is denoted as m-S (n-PCMEU)A (serial-parallel-connected ME unit array). To form a magnetic sensor, as demonstrated in Fig. 2, the m-S (n-PCMEU)A is assembled by mounting four single 2-PCMEUs ($m = 4$ and $n = 2$) on the walls of a solid plastic housing and inserted into an excitation solenoid coil, which can be space-saved.

The experimental setup for ME effect measurements is presented in Fig. 2. In this setup, a homogenous DC magnetic field created by a Helmholtz coil (MH-2.5, Lake Shore Cryotronics, Inc) is driven by a Keithley 2400, ranging from −1 A to 1 A with a resolution of 10 μA. The ME composite operation is excited by an AC magnetic field, $h_{ac} = 1.74 \times 10^{-2}$ Oe, generated by an excitation solenoid coil with a diameter of 60 mm and 16,667 turns per meter that is driven by the Lock-in amplifier 7265 (Ametek Scientific Instruments, Pennsylvania, USA). The ME voltage signal V_{ME} is finally measured by the same Lock-in amplifier and the ME voltage coefficient α_E was determined by $\alpha_E = V_{ME}/(t_p.h_{ac})$.

3. Results and discussion

3.1. ME geometrics simulation design

As mentioned above, the ME output voltage appearing in PZT layer caused by the magnetic field induced strain or stress of Metglas layers. Indeed, the (force) magnetostriction is almost quadratically proportional to the magnetization M (and thus, the magnetic flux density or magnetic induction B) of the magnetic phase, i.e., $\lambda \sim M^2$ [21]. The ME geometrics simulation design can, therefore, partly be understood through the information of the magnetic flux distribution on the Metglas substance. In this section, the simulation is performed using the magnetization response of Metglas layers as the input parameters in the Magnetostatic mode [17] and the finite element method Ansys Maxwell 3D (Version 16, USA) as a computational tool.

The $B(H)$ data of Metglas are collected by VSM (model 731, Lakeshore Cryotronics, Inc., Westerville, OH, USA). In the simulation, a homogeneous DC magnetic field of 0.4 Oe was set in the simulation region, along the length of the ME unit. This field is equivalent to the horizontal component of the earth's magnetic field. The effective magnetic flux taken over the Metglas volume $B_{eff} = \frac{1}{V}\int BdV$ was used to predict different ME composite geometries under investigation, consisting of the conventional single bar (*c*-SB), conventional separate multi-bar (*c*-SMB), elongated separate multi-bar (*e*-SMB) and *n* magnetic bars based parallel-connected-multi-bars n-PCMB with variable conjoined end's length from $c = 1$–5 mm.

The (simulated) magnetic flux distribution on the Metglas layers and the magnetic flux density are presented in Fig. 3a and b, respectively. In general, the magnetic flux is strongly concentrated at the bar center and attenuated at the two ends. Compared with the conventional single bar (c-SB), the magnetic flux density in the separate 2-bar configuration with the same length (c-SMB n = 2) is almost reserved. The effective magnetic flux density calculated over the whole c-SMB sample is 24.26 mT, only 1.7% lower than the value of 24.69 mT in *c*-SB sample. This permits to neglect the demagnetization effect caused by neighboring (adjacent) bars. However, the large inhomogeneity of the magnetic flux still remains in both cases. As can be seen from Fig. 3b, the B strongly decreases starting from the position $|x/L_s| = 0.5$ and is almost annulled (with $B\ (x = L_s) = 2.17$ mT) at the two bar ends leading to a very high magnetic inhomogeneity of the magnetic flux density. In order to estimate the inhomogeneity of the magnetic flux density, the relative reduction ratio of B_{eff} from the center to the bar ends of the sensing part is given by:

$$r = \frac{\Delta B}{B_{max}} = \frac{B(x=0) - B(x=L_s)}{B(x=0)}$$

This ratio, as obtained from the simulation, results for the c-SB sample to a value for r of 93%.

To improving the magnetic homogeneity of this magnetic flux distribution, the Metglas bars are elongated at both ends. Indeed, the relative reduction ratio r is only 17% for the elongated separate multi-bar (*e*-SMB) with $n = 2$ and elongated length of $e = 5$ mm. An even better homogeneity with $r = 6\%$ can be obtained for the configuration of parallel-connected-multi-bars 2-PCMB with $e = c = 5$ mm. In this case, the effective magnetic flux density reaches the highest value of 26.14 mT. The simulations for different n-PCMB samples showed that although the B_{eff} value is slightly reduced less than 2% when increasing the number of bars from $n = 2$ to 6 by demagnetization effect, the relative reduction ratio r is kept almost no change. The simulated geometries are experimentally implemented and the results are presented below.

3.2. Experimental implementation

The dependence of the ME voltage signal on the AC magnetic-field frequency measured at a fixed DC magnetic field is presented in Fig. 4a for the ME geometries of c-SB, c-SMB and n-PCMB (n = 2). The results show that the resonance appears at resonant frequencies (f_r) ranging between 32.75 and 33 kHz. This finding is in good agreement with the reported in [7] that for ME laminates having $L >> W$, the resonant frequency is mainly governed by the length of the piezoelectric layer: $f_r \sim 1/L_s$.

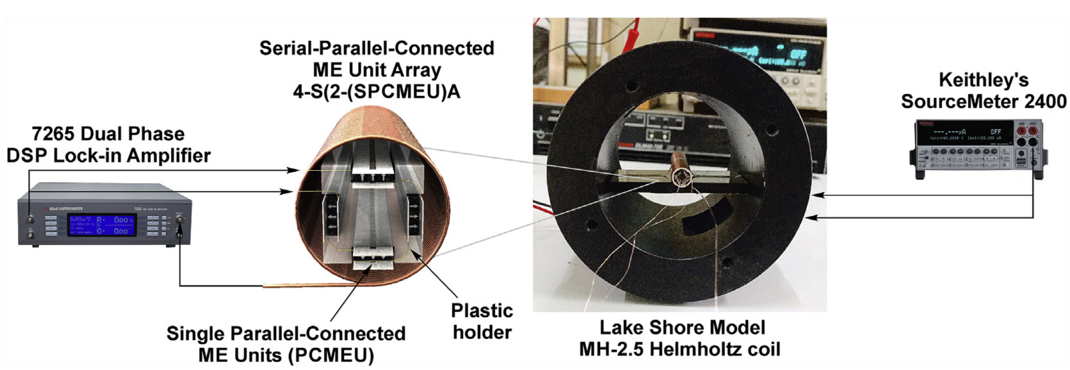

Fig. 2. Experimental setups for serial-parallel ME unit array of 4-S (2-PMEU)A and ME voltage response measurement setup.

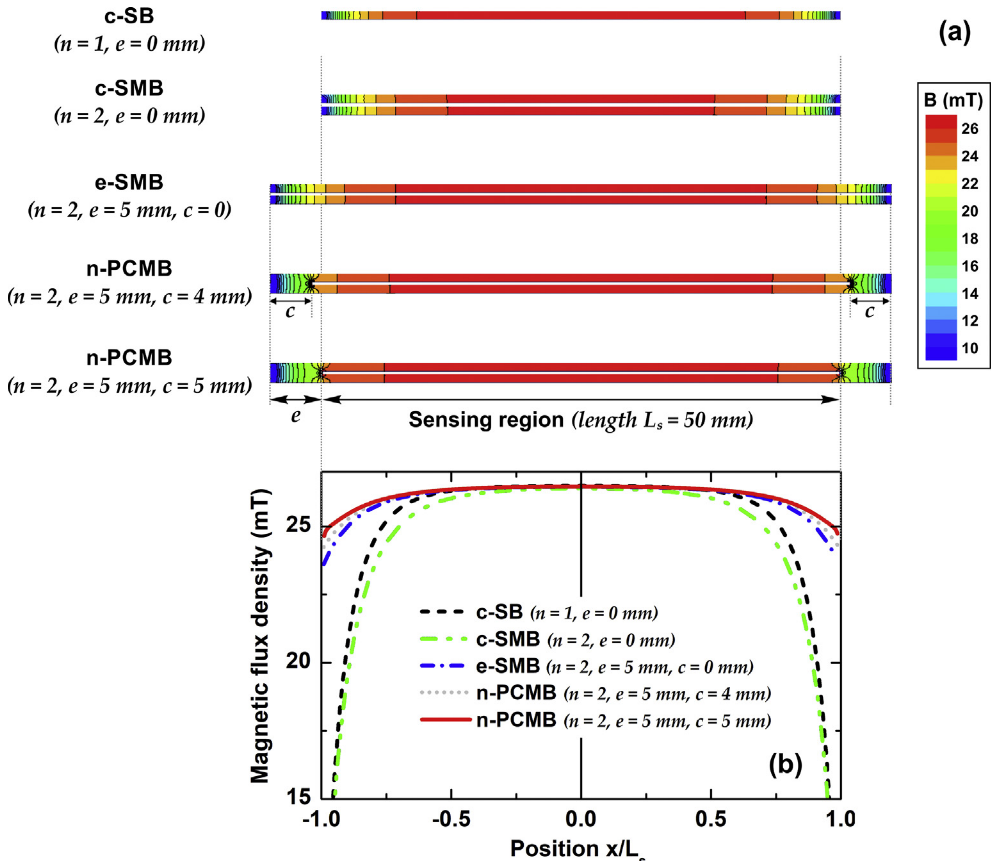

Fig. 3. Simulated magnetic flux (a) and magnetic flux density distribution (b) along the length plotted in the sensing region obtained for the conventional single bar (*c*-SB), conventional separate multi-bar (*c*-SMB), elongated separate multi-bar (*e*-SMB), parallel-connected-multi-bars n-PCMB ($n = 2$) with different length of the conjoined part.

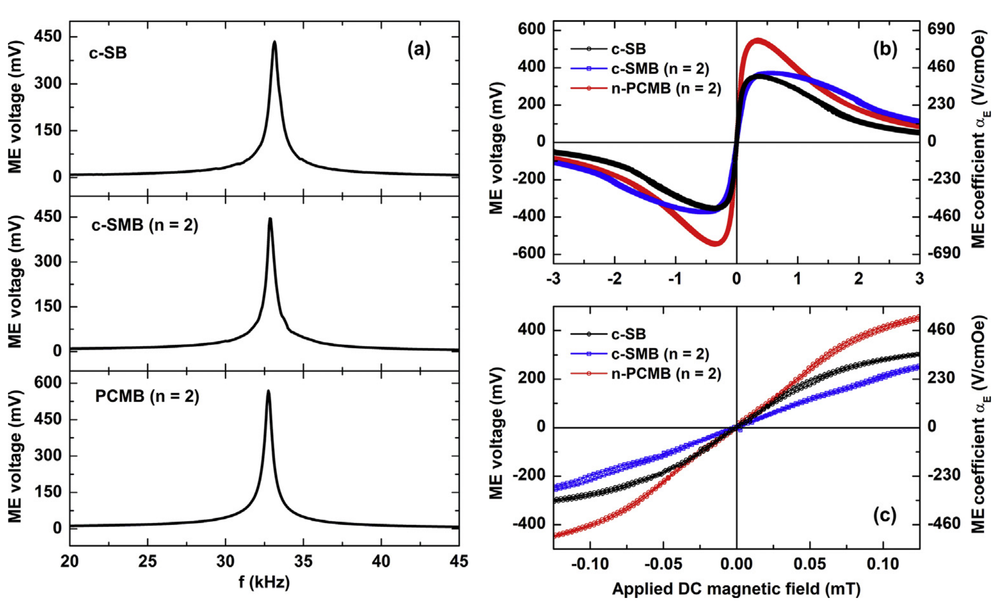

Fig. 4. The magnetoelectric voltage response scanning to the frequency (a), the ME voltage and ME voltage coefficient versus applied DC magnetic fields measured at the resonant frequency plotted in full range (b) and small range (c) for different sample c-SB, c-SMB and n-PCMB (n = 2).

The ME voltage versus the applied DC magnetic field, plotted in full range (Fig. 4b) and in a small range (Fig. 4c), exhibits the advantages of the PCMB with respect to the c-SB geometry at both low and high applied magnetic fields. Indeed, the results show the highest low-field ME voltage response as well as the highest sensitivity represented by the curve's slope in comparison with others for PCMB. The ME voltage coefficient α_E, as high as 629.9 mV/cm.Oe in PCMB, is increased by a factor of 1.47 with respect to the

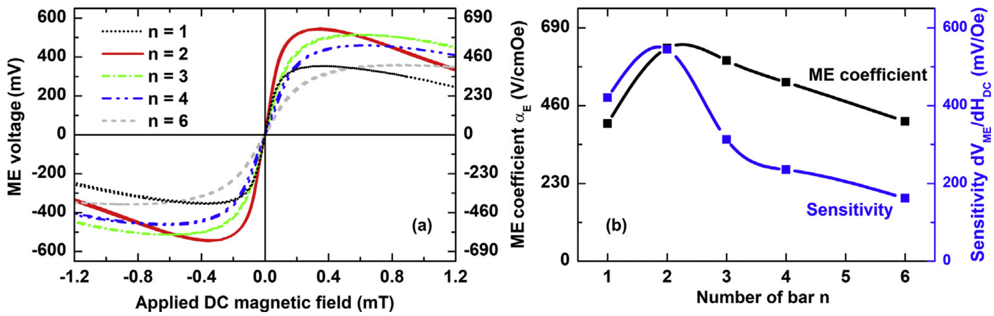

Fig. 5. The magnetoelectric voltage response to applied magnetic fields (a) and maximal ME voltage and sensitivity in n-PCMB geometries with different numbers of bars $n = 1, 2, 3, 4$, and 6 (b).

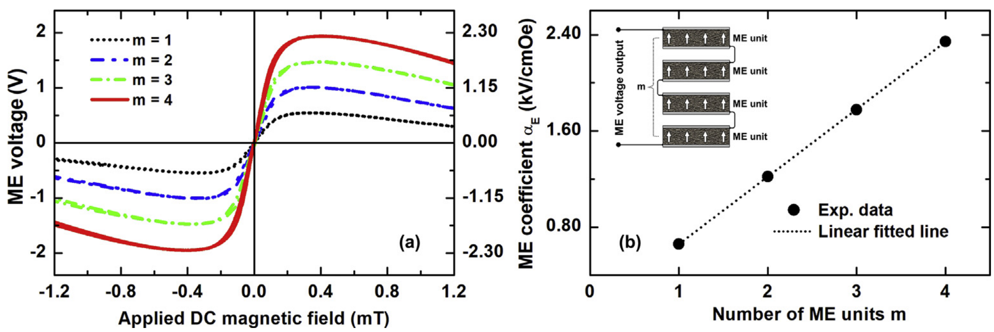

Fig. 6. Magnetoelectric voltage response to the applied magnetic field (a) and maximal ME voltage recorded at resonant frequency (b) measured in the 4-S (2-PCMEU)A array with a different number m of ME units.

value of 427.6 V/cm.Oe in the c-SB sample. Furthermore, the magnetic field range at which α_E does not reach its maximal value in PCMB is extended to higher magnetic fields in comparison with that of c-SB. For the c-SMB geometry, a worse ME performance is observed at low magnetic fields, while ME voltage response and ME coefficient are somewhat increased at high fields. This reflects the fact that the combination of both the attenuation of the shear-lag effect in the large PZT plate and the enhancement of the magnetic softness in the narrowed Metglas bar in c-SMB is still insufficient to improve the ME performance. Here, besides the magnetic flux inhomogeneity, the reason for it may also be attributed to the decrease of the piezomagnetic/piezoelectric volume fraction caused by the existence of gaps between bars in c-SMB geometries. As can be seen below, this rule is further reinforced in n-PCMB units with high number $n > 2$.

The ME effect characterization versus applied DC magnetic fields measured for PCMB geometries with different number of bars of $n = 1$ (SB) to 6 is presented in Fig. 5a. The ME voltage coefficient and the sensor sensitivity extracted from the ME voltage curve's slope are plotted as a function of the number of bars n in Fig. 5b. In this PCMB series, the strong magnetic flux is confirmed to be homogeneous over the whole range of the sensing length. However, the optimal ME performance is reached at $n = 2$ with the largest maximal ME voltage coefficient $\alpha_E = 629.9$ V/cm.Oe. This value is still far from the giant ME coefficient of 5 kV/cm Oe in thin film structures [22] but it is 1.26 times larger than the highest value $\alpha_E = 500$ V/cm.Oe found in FeBSiC/piezofiber layered composites [9]. With increasing number of bars, n > 2, the ME maximum shifts to higher applied magnetic fields, but the maximal ME voltage and the sensitivity decrease. Similarly, this observation can also be attributed to the decrease of the piezomagnetic/piezoelectric volume fraction in PCMB units when increasing n.

To develop integrated serial-parallel ME unit arrays, a number m of single ME units in the 2-PCMB ($n = 2$) geometry is chosen, connected to form m-S (2-PMEU)A arrays and tested in turn with $m = 1, 2, 3$ and 4. The ME voltage response and the corresponding ME coefficient α_E are illustrated in Fig. 6a. The maximum value of α_E is plotted *vs* the number m of single ME units as shown in Fig. 6b. It can be clearly seen that the behavior of the ME voltage signal as well as the ME voltage coefficient are quite similar for all m. Only the value is multiplied, *i.e.* the ME voltage coefficient and the sensor's sensitivity proportionally increases with the number of single ME units integrated in the array. The value for α_E increases 3.6 times from 630 V/cm.Oe to 2.238 kV/cm.Oe when the number of ME units increases from $m = 1$ to 4 respectively. These results demonstrate that the sensitivity enhancement can be found not only in the PCMB ($n = 2$) geometry, but also in the novel integrated serial-parallel PZT/Metglas array m-S (2-PMEU)A.

To estimate the sensitivity and the resolution of the m-S (n-PMEU)A for low-magnetic-field sensor applications, the data recorded at small fields ranging from 0 to 3000 nT and the real-time output signal in response to the variation in steps of 50 nT of the incident DC magnetic fields are shown in Fig. 7a and Fig. 7b, respectively. It is clearly seen that the ME voltage responses perfectly depend linearly on the applied fields. A huge sensitivity of 18.1 μV/nT is achieved in the 4-S (2-PCMEU)A with 4 single ME units. This value is nearly 4 times higher than that of 5 μV/nT in a single PCMB unit. This sensitivity can even be increased simply by increasing the AC excited magnetic field strength due to the output ME voltage is linearly proportional with h_{ac} [23,24].

To estimate the noise contribution of the SPMEUA, the sensor stability in an invariant magnetic field of 1000 nT was performed in a time period of 5 min. The results are given in Fig. 8a. The Fig. 8b provides the statistical histogram of the output voltage,

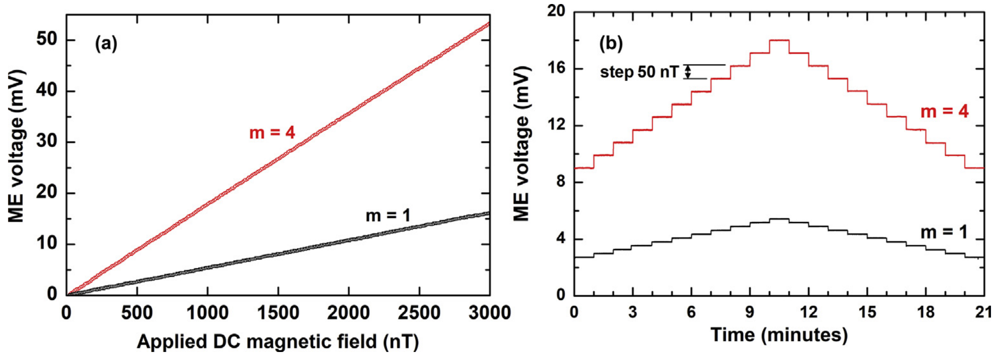

Fig. 7. (a) Magnetoelectric voltage response to low magnetic fields and (b) and real-time measurement results for different tiny steps of the magnetic field of 10 nT in the magnetic field range from 500 to 1000 nT for sensors using $m = 1$ and 4 of 2-PCMEUs.

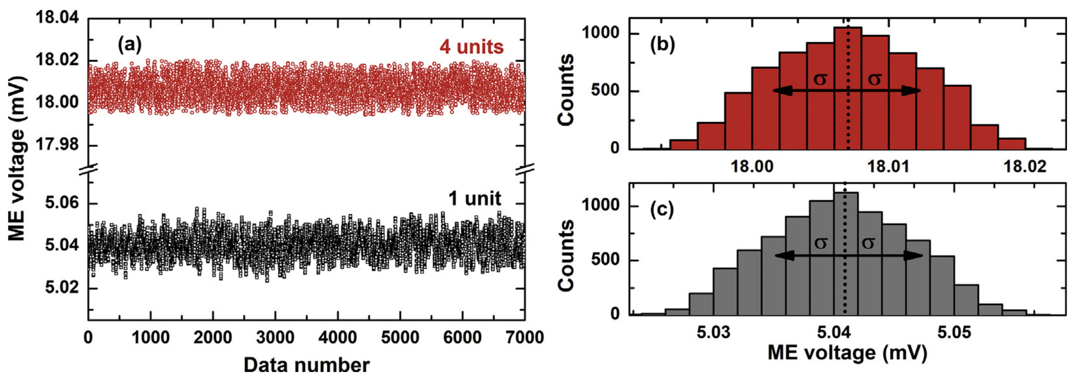

Fig. 8. Sensor stability measured in an invariant magnetic field of 1000 nT recorded in the period of time of 5 min for 7000 data points (a) and the statistical histogram of the output voltage in m-S (2-PCMEU)A sensors of different numbers of ME unit $m = 4$ (b) and 1 (c).

which is governed by a normal distribution. The accuracy of the sensor array is estimated from the standard deviation (σ) value of about 0.0058 and 0.0053 mV within 7000 averaged data points in sensor PSMEUA array of $m = 4$ (Fig. 8b) and $m = 1$ (Fig. 8c) ME units, respectively. These results showed that the noise background is almost the same. As a result, the signal to noise S/N ratio is increased by nearly the same factor as the number of ME units integrated with the m-S (n-PCMEU)A array thanks to the increase of ME voltage signal. From this accuracy and its sensitivity, the resolution of 10^{-1} nT was estimated in the m-S (n-PMEU)A sensor measuring in environmental conditions.

4. Conclusion

This paper describes the route, from simulation towards experiment, for optimizing ME geometries with multiplied ME voltage responses. This is structured with the design of a parallel-connected-multi-bars (PCMB) geometry of the magnetic phase in simple PZT/Metglas composites, in which not only the huge magnetostrictive softness and high homogeneity, but also a decreased shear-lag effect and a space-saving construction are ensured. The magnetic n-PCMB geometry with n magnetic narrowed bars divides the conventional ME composites into n parallel-connected ME units (n-PCMEU). In addition, m of these n-PCMEUs can be further serially connected to form an m-S (n-PCMEU)A array. For the n-PCMEU geometries, the optimal ME composite with the largest ME voltage coefficient $\alpha_E = 630$ V/cm.Oe is found with $n = 2$. For m-S (n-PCMEU)A, the ME voltage coefficient turns out to be almost proportional to m. Indeed, α_E increases by a factor of 3.6 to the value of 2.238 kV/cm.Oe for 4-S (2-PCMEU)A. The corresponding m-S (n-PCMEU)A sensor exhibits the huge sensitivity of 18.1 μV/nT and a resolution of 10^{-1} nT.

Declaration of Competing Interest

The authors declare that they have no known competing financial interests or personal relationships that could have appeared to influence the work reported in this paper.

Acknowledgement

This work was supported by Vietnam National Research Program under the granted Research Project No. ĐTĐL.CN - 02/17.

References

[1] Y. Shen, J. Gao, Y. Wang, J. Li, D. Viehland, Thermal stability of magnetoelectric sensors, Appl. Phys. Lett. 100 (2012) 2012–2015, https://doi.org/10.1063/1.4705298.

[2] F. Fang, Y.T. Xu, W. Yang, Magnetoelectric coupling of laminated composites under combined thermal and magnetic loadings, J. Appl. Phys. 111 (2012), https://doi.org/10.1063/1.3677945.

[3] D.A. Burdin, N.A. Ekonomov, D.V. Chashin, L.Y. Fetisov, Y.K. Fetisov, M. Shamonin, Temperature dependence of the resonant magnetoelectric effect in layered heterostructures, Materials 10 (2017) 1–19, https://doi.org/10.3390/ma10101183.

[4] Y. Wang, S.W. Or, H.L.W. Chan, X. Zhao, H. Luo, Enhanced magnetoelectric effect in longitudinal-transverse mode Terfenol-D/Pb (Mg1/3Nb2/3) O3-PbTiO3 laminate composites with optimal crystal cut, J. Appl. Phys. 103 (2008) 2–6, https://doi.org/10.1063/1.2943267.

[5] N.H. Duc, D.T.H. Giang, Magnetic sensors based on piezoelectric-magnetostrictive composites, J. Alloys Compd. 449 (2008), https://doi.org/10.1016/j.jallcom.2006.01.121.

[6] D. Hasanyan, J. Gao, Y. Wang, R. Viswan, M. Li, Y. Shen, J. Li, D. Viehland, Theoretical and experimental investigation of magnetoelectric effect for

bending-tension coupled modes in magnetostrictive-piezoelectric layered composites, J. Appl. Phys. 112 (2012), https://doi.org/10.1063/1.4732130.
[7] D.T.H. Giang, P.A. Duc, N.T. Ngoc, N.H. Duc, Geomagnetic sensors based on Metglas/PZT laminates, Sensors Actuators, A Phys. 179 (2012) 78–82, https://doi.org/10.1016/j.sna.2012.03.030.
[8] J. Zhai, Z. Xing, S. Dong, J. Li, D. Viehland, Detection of pico-Tesla magnetic fields using magneto-electric sensors at room temperature, Appl. Phys. Lett. 88 (2006) 5–8, https://doi.org/10.1063/1.2172706.
[9] S. Dong, J. Zhai, J. Li, D. Viehland, Near-ideal magnetoelectricity in high-permeability magnetostrictive/piezofiber laminates with a (2-1) connectivity, Appl. Phys. Lett. 89 (2006) 2–5, https://doi.org/10.1063/1.2420772.
[10] E. Freeman, J. Harper, N. Goel, I. Gilbert, J. Unguris, S.J. Schiff, S. Tadigadapa, Improving the magnetoelectric performance of Metglas/PZT laminates by annealing in a magnetic field, Smart Mater. Struct. 26 (2017), 085038, https://doi.org/10.1088/1361-665x/aa770b.
[11] Y. Shen, K.L. McLaughlin, J. Gao, M. Li, J. Li, D. Viehland, Effective optimization of magnetic noise for a Metglas/Pb(Zr,Ti)O 3 magnetoelectric sensor array in an open environment, Mater. Lett. 91 (2013) 307–310, https://doi.org/10.1016/j.matlet.2012.10.003.
[12] X. Liang, C. Dong, H. Chen, J. Wang, Y. Wei, M. Zaeimbashi, Y. He, A. Matyushov, C. Sun, N. Sun, A review of thin-film magnetoelastic materials for magnetoelectric applications, Sensors 20 (2020) 1532, https://doi.org/10.3390/s20051532.
[13] M. Bichurin, V. Petrov, R. Petrov, A. Tatarenko, V. Leontiev, Journal of magnetism and magnetic materials nomograph method for predicting magnetoelectric coupling, J. Magn. Magn Mater. 412 (2016) 1–6, https://doi.org/10.1016/j.jmmm.2016.03.070.
[14] J. Das, J. Gao, Z. Xing, J.F. Li, D. Viehland, Enhancement in the field sensitivity of magnetoelectric laminate heterostructures, Appl. Phys. Lett. 95 (2009), 092501, https://doi.org/10.1063/1.3222914.
[15] C.S. Park, C.W. Ahn, J. Ryu, W.H. Yoon, D.S. Park, H.E. Kim, S. Priya, Design and characterization of broadband magnetoelectric sensor, J. Appl. Phys. 105 (2009) 1–7, https://doi.org/10.1063/1.3117484.
[16] M. Bichurin, V. Petrov, A. Tatarenko, Predicting magnetoelectric coupling in layered and graded composites, Sensors 17 (2017) 1651, https://doi.org/10.3390/s17071651.
[17] D.T. Huong Giang, P.A. Duc, N.T. Ngoc, N.T. Hien, N.H. Duc, Enhancement of the magnetic flux in Metglas/PZT-Magnetoelectric integrated 2D geomagnetic device, Jpn. Mag. 17 (2012) 308–315, https://doi.org/10.4283/JMAG.2012.17.4.308.
[18] D.T. Huong Giang, P.A. Duc, N.T. Ngoc, N.T. Hien, N.H. Duc, Spatial angular positioning device with three-dimensional magnetoelectric sensors, Rev. Sci. Instrum. 83 (2012), https://doi.org/10.1063/1.4752763.
[19] C.M. Chang, G.P. Carman, Modeling shear lag and demagnetization effects in magneto-electric laminate composites, Phys. Rev. B Condens. Matter 76 (2007) 1–7, https://doi.org/10.1103/PhysRevB.76.134116.
[20] https://www.americanpiezo.com/apc-materials/physical-piezoelectric-properties.html (accessed March 15, 2020).
[21] A. Clark, Ferromagnetic Materials, North Holland Publishing, Amsterdam, The Netherlands, 1980.
[22] C. Kirchhof, M. Krantz, I. Teliban, R. Jahns, S. Marauska, B. Wagner, R. Knöchel, M. Gerken, D. Meyners, E. Quandt, Giant magnetoelectric effect in vacuum, Appl. Phys. Lett. 102 (2013), https://doi.org/10.1063/1.4810750.
[23] D.T.H. Giang, N.H. Duc, Magnetoelectric sensor for microtesla magnetic-fields based on (Fe80Co20)78Si12B10/PZT laminates, Sensors Actuators, A Phys. 149 (2009) 229–232, https://doi.org/10.1016/j.sna.2008.12.003.
[24] D.T. Huong Giang, L.K. Quynh, N. Van Dung, N.H. Nghi, Magnetoelectric effects in piezoelectric/soft magnetic amorphous FeCo-based ribbon composites, J. Phys. Conf. Ser. 187 (2009) 6–11, https://doi.org/10.1088/1742-6596/187/1/012057.